Acta Biomaterialia 75 (2018) 200–212

Contents lists available at ScienceDirect

Acta Biomaterialia

journal homepage: www.elsevier.com/locate/actabiomat

Full length article

# 3D breast cancer microtissue reveals the role of tumor microenvironment on the transport and efficacy of free-doxorubicin *in vitro*

Virginia Brancato [a,1], Filomena Gioiella [a,1], Giorgia Imparato [b], Daniela Guarnieri [b,d], Francesco Urciuolo [b,*], Paolo A. Netti [a,b,c]

[a] Interdisciplinary Research Centre on Biomaterials (CRIB), University of Napoli Federico II, P.le Tecchio 80, 80125 Napoli, Italy
[b] Center for Advanced Biomaterials for Health Care@CRIB, Istituto Italiano di Tecnologia, Largo Barsanti e Matteucci 53, 80125 Napoli, Italy
[c] Department of Chemical, Materials and Industrial Production Engineering (DICMAPI), University of Napoli Federico II, P.le Tecchio 80, 80125 Napoli, Italy
[d] Nanobiointeractions & Nanodiagnostics, Istituto Italiano di Tecnologia (IIT), Via Morego, 30, 16163 Genova, Italy

ARTICLE INFO

*Article history:*
Received 18 October 2017
Received in revised form 21 May 2018
Accepted 31 May 2018
Available online 1 June 2018

*Keywords:*
3D breast cancer model
Extracellular matrix
Microtissues
Doxorubicin

ABSTRACT

The use of 3D cancer models will have both ethical and economic impact in drug screening and development, to promote the reduction of the animals employed in preclinical studies. Nevertheless, to be effective, such cancer surrogates must preserve the physiological relevance of the *in vivo* models in order to provide realistic information on drugs' efficacy. To figure out the role of the architecture and composition of 3D cancer models on their tumor-mimicking capability, here we studied the efficacy of doxorubicin (DOX), a well-known anticancer molecule in two different 3D cancer models: our 3D breast cancer microtissue (3D-μTP) versus the golden standard represented by spheroid model (sph). Both models were obtained by using cancer associated fibroblast (CAF) and breast cancer cells (MCF-7) as cellular component. Unlike spheroid model, 3D-μTP was engineered in order to induce the production of endogenous extracellular matrix by CAF. 3D-μTP have been compared to spheroid in mono- (MCF-7 alone) and co-culture (MCF-7/CAF), after the treatment with DOX in order to study cytotoxicity effect, diffusional transport and expression of proteins related to cancer progression. Compared to the spheroid model, 3D-μTP showed higher diffusion coefficient of DOX and lower cell viability. Also, the expression of some tumoral biomarkers related to cell junctions were different in the two models.

**Statements of Significance**

Cancer biology has made progress in unraveling the mechanism of cancer progression, anyway the most of the results are still obtained by 2D cell cultures or animal models, that do not faithfully copycat the tumor microenvironment. The lack of correlation between preclinical models and *in vivo* organisms negatively influences the clinical efficacy of chemotherapeutic drugs. Consequently, even if a huge amount of new drugs has been developed in the last decades, still people are dying because of cancer. Pharmaceutical companies are interested in 3D tumor model as valid alternative in drug screening in preclinical studies. However, a 3D tumor model that completely mimics tumor heterogeneity is still far to achieve. In our work we compare 3D human breast cancer microtissues and spheroids in terms of response to doxorubicin and drug diffusion. We believe that our results are interesting because they highlight the potential role of the proposed tumor model in the attempts to improve efficacy tests.


## 1. Introduction

Pharmaceutical companies have been facing a huge burden, both financially and clinically, because of the shortage of adequate *in vitro* models that could make more reliable the preclinical studies to test drug efficacy. In the last decades, only about 5% of cancer drug candidates that enter clinical trials received approval from the U.S. Food and Drug Administration. Anti-cancer drug validation

*Abbreviations:* TME, tumor microenvironment; ECM, extracellular matrix; DOX, doxorubicin; GPMs, gelatin porous microbeads; GAL, glyceraldehyde; RT, room temperature; CAF, carcinoma associated fibroblasts; MCF7, human breast adenocarcinoma cells; Sph, spheroid/spheroids; 3D-μTP, three dimensional microtissue precursor/precursors.

* Corresponding author.
*E-mail address:* urciuolo@unina.it (F. Urciuolo).
[1] These authors equally contributed to the work.

https://doi.org/10.1016/j.actbio.2018.05.055
1742-7061/

screening is still performed on two dimensional (2D) cell culture systems as multiwell plates [1]. 2D cells cultures can be perfectly adapted to high throughput screening approach used in the preclinical studies and offered a fast, relatively low-cost approach for drug screening. Moreover the handling procedure for 2D cell cultures is quite easy and reproducible. However, 2D cells cultures showed some limits since they are deprived of two key factors showed in tumor tissues such as extracellular matrix (ECM), a fundamental component in regulating tumor progression [2] and three dimensional (3D) arrangement. As a consequence, although 2D systems are useful models for fast discovering of crucial molecular pathways, its prediction potential of the *in vivo* response is controversial [3]. On the other hand, animal testing in clinical research should be limited since their use is time-consuming, expensive and poorly predictive of human response to drug [4].

In the last decades the attention moved on alternative preclinical study models that could be able to copycat the complexity of tissues and in particular tumor microenvironment. So far, different *in vitro* tumor models have been developed in order to improve the prediction potential of the testing [5]. Among these models, 3D culture systems offer the unique opportunity to culture cancer cells in a spatially relevant manner, encouraging cell-cell and cell-matrix interactions that closely mimic the native tumor environment [5,6]. Spheroid is one of the most common and versatile 3D cancer models since it recapitulates the *in vivo* tumor architecture [7]. Several studies have demonstrated the simplicity and high reproducibility of the spheroid model, making it suitable as drug screening platform [8,9]. However, spheroids have some limitations since they are compact cell aggregates that do not interact with their extracellular milieu and do not have physical resistance provided by the ECM [2,10–12]. Beside the ECM, the presence of different type of cells is relevant in order to improve the similarity between *in vitro* models and *in vivo* tumor. ECM and stroma cells like fibroblasts, endothelial cells and immune system cells, are involved in the mechanisms triggering the tumor development. Nevertheless, only few works reported the incorporation of stromal cells in spheroid models [13–18]. Therefore, many efforts should be done in order to reproduce a more relevant tumor model recapitulating 3D cell architecture, multiple cell types and ECM [13]. In addition, in a previous work it has been proved that 3D arrangement alone did not guarantee the replication of tumor physiology *in vitro* unless cells have produced and assembled their own tumor ECM [19]. In this direction, microcarriers based approach have been employed to guide cell development into 3D organization to better mimic the native tissue, providing a more reliable tool for drug testing [20–22]. Differently to the spheroid approach, in cell-seeded microcarrier systems cells have been induced to grow both on the microbeads surface and in the inner porosity. Under controlled culture conditions, cells seeded into microbeads synthesize and assemble their own ECM. For this reason the microcarriers based approach have led to a more realistic tumor tissue model for *in vitro* applications such as drug testing [19,23–25]. In this scenario, by comparing two different breast cancer models - 3D spheroids versus 3D-μTP – we elucidated the role of 3D arrangement in affecting cytotoxic effects/therapeutic efficacy of doxorubicin (DOX) [26]. Both models have been obtained by using breast cancer cell line (MCF-7) in either mono-culture or in co-culture with cancer-associated fibroblasts (CAF). 3D-μTP have been fabricated by seeding tumor and/or fibroblast cells into porous biodegradable microcarriers in a dynamic culture system according to our previous works [21,22]. We found that the two 3D cancer models behaved differently in terms of response to DOX regardless to the cell composition (mono-culture or co-culture). We related these differences to the different features of the 3D cancer models. Indeed, spheroids showed a higher cell density and were poor in cell-assembled ECM compared to both 3D-μTP and xenograft. The highest cell density found in the spheroid resulted in a high density of cell-cell junctions that affected the transport of DOX across the bulk of the spheroid model resulting in a lower diffusion coefficient than the 3D-μTP.

## 2. Materials and methods

### 2.1. Cell type

Cancer associated fibroblasts (CAF) were provided by the group of prof. Bussolino (IRCCS Institute of Candiolo, Turin, Italy) following the procedures previously described [27,28]. Stable transfected CAF with pLVX-DsRed-express2-N1 ($\lambda_{ex}$ 554 nm, $\lambda_{em}$ 591 nm) viral vector (Clontech, USA) were also used to distinguish them in the cell counting in coculture (data not shown). To avoid fluorescence overlapping, not-transfected CAF cells have been used for immunofluorescence analysis. Cells were sub-cultured onto 150 mm Petri dishes in DMEM (Dulbecco's Modified Eagle Medium) with high glucose, containing 10% fetal bovine serum, 100 μg/ml L-glutamine and 100 U/ml penicillin/streptomycin. Human breast adenocarcinoma cells (MCF7) kindly donated by Daidone's group, were sub-cultured onto 150 mm Petri dishes in RPMI-1640 (Roswell Park Memorial Institute) containing 10% fetal bovine serum, 100 μg/ml L-glutamine and 100 U/ml penicillin/streptomycin. Cells were maintained at 37 °C in humidified atmosphere containing 5% $CO_2$.

### 2.2. Microbeads production

Gelatin porous microbeads (GPMs) were prepared according to a previously described [22] double emulsion technique (O/W/O). All the materials were purchased at Sigma Aldrich Chemical Company. Briefly, gelatin type B (Bloom 225, Mw ¼ 176.654 Da) was dissolved into 10 ml of water containing TWEEN 85 (6% w/v). The solution was kept at 40 °C. Toluene containing SPAN 85 (3% w/v) was continuously added to the aqueous gelatin solution (8% w/v) to obtain primary oil in water emulsion. The added toluene formed droplets in the gelatin solution until saturation. Beads of gelatin containing droplets of toluene were produced through the addition of excess toluene (30 ml) that allowed for a double emulsion (O/W/O). After cooling below 5 °C, 20 ml of ethanol were added to extract toluene and stabilize GPMs. The resulting microspheres were filtered and washed with acetone and then dried at room temperature. Microspheres were separated selectively by using commercial sieves (Sieves IG/3-EXP, Retsch, Germany). GPMs with 75 ÷ 150 μm size range were recovered and further processed. GPMs were stabilized by means of chemical treatment with 5% glyceraldehyde (GAL). In particular, GPMs were dispersed into an acetone/water solution containing 5% GAL and mixed at 4 °C for 24 h. Then microspheres were washed with acetone and dried at RT. As analyzed in previous paper [22], GPMs had spherical shape, their mean internal pore size was 10–20 μm and pores were well interconnected to allow the seeding and spreading of the cells throughout the scaffold.

### 2.3. Dynamic cell seeding

Before using, dry GPM were sterilized in absolute ethanol 24 h on a rotating plate. Then, GPMs were washed twice in sterile phosphate-buffered saline (PBS) without calcium and magnesium solution. Finally, before cell seeding, PBS was replaced by fresh culture medium. For homotypic microtissues, MCF7 cells were seeded onto 50 mg of GPMs in a 30 cell/GPM ratio. To help cell seeding on GPMs an intermittent stirring regime (30 min at 0 rpm, 5 min at 30 rpm) for 6 h was performed. Then, dynamic cultures were kept

under continuous stirring at 30 rpm for up to 12 days. For heterotypic culture (CAF/MCF7-μTP), at day 6, MCF7 cells were added in a ratio 1:3 to CAF cells into a spinner flask. Medium was changed the first day and every 3 days until the end of the experiments. From the day 2, 50 μg/ml of ascorbic acid were added to CAF/MCF7-μTP.

### 2.4. Homotypic and heterotypic spheroid formation

For spheroid formation a previously published procedure was followed [29]. Briefly, MCF-7 cells were trypsin-treated and counted. Subsequently, they were seeded onto round bottom non-tissue culture treated 96 well-plates (Falcon, BD NJ, USA) at a concentration of 2500 cells/well in RPMI 10% FCS supplemented with 20% methylcellulose stock solution. For co-cultured spheroids, we used a total of 2500 cells/well, where CAF were seeded in a ratio 3:1 with MCF7 cells. For preparation of methylcellulose stock solution, 3 g of methylcellulose powder (M0512, Sigma-Aldrich) were autoclaved in a 250 ml bottle containing a magnetic stirrer. The autoclaved methylcellulose was dissolved in preheated 125 ml basal medium (60 °C) for 20 min. Thereafter, 125 ml medium containing double amount of FCS (20%) was added to a final volume of 250 ml and the whole solution mixed overnight at 4 °C. The final stock solution was aliquoted and cleared by centrifugation (5000*g*, 2 h, RT). Only the clear highly viscous supernatant was used for the spheroid assay (about 90–95% of the stock solution). For spheroid generation was used 0.24% methylcellulose as final concentration. Spheroids were grown under standard culture conditions (5% $CO_2$, at 37 °C) and harvested at different time points for further investigations. From the day 2, 50 μg/ml of ascorbic acid were added to CAF/MCF7-sph.

### 2.5. Drug treatment and cytotoxicity

To have a cell density of about 2500 cells in each well of the 96-well plate and perform the drug testing, we transferred one CAF/MCF7-μTP/well and about 50 MCF7-μTP (we took 1 ml of MCF7-μTP suspension from the spinner flask and counted the microtissues). Both spheroids and μTP were treated with free DOX (Sigma) at 4, 8 and 16 μg/ml. After the DOX treating for 48 and 72 h at 37 °C and 5% $CO_2$, the medium was removed and 200 μL of 3-(4,5-dimethylthiazol-2-yl)-2,5-diphenyltetrazolium bromide (MTT) solution (5 mg/ml) was added to each well. After 4 h incubation that allows the viable cells to reduce the yellow MTT into dark-blue formazan crystals, 100 μL of dimethyl sulfoxide (DMSO) were added to each well and incubate for 1 h. The absorbance of individual well was measured at 595 nm by a microplate reader (Enspire Multimode Plate Reader PerkinElmer). All experiments were performed in triplicates.

### 2.6. Fluorescence imaging

μTP and spheroids treated with DOX were washed three times with PBS and fixed in 4% paraformaldehyde (PFA) in PBS for 20 min. Cell nuclei were stained with 1 μg/ml 4′,6-diamidino-2-phenylindole (DAPI , Sigma-Aldrich) as described previously [19].

DOX fluorescence was observed by means of a confocal microscope (Leica) with $\lambda_{ex}$ = 490 nm and $\lambda_{em}$ = 530 nm and with a 40X water objective (NA = 1.10). DAPI were acquired by setting $\lambda_{ex}$ = 700 (two photon) nm and $\lambda_{em}$ = 400/450 nm.

### 2.7. Diffusion measurement by fluorescence recovery after photobleaching (FRAP)

DOX Diffusion was measured with fluorescein isothiocyanate with similar molecular weight (389.38 g/mol, Sigma) by Fluorescence Recovery After Photobleaching (FRAP) technique, as used in our previous work [25]. Briefly, FRAP measurements were conducted with a laser scanning microscope (TCS SP5, Leica) using a 25X (NA = 0.95) objective and a 488 nm excitation line from Argon laser operating with 5% output power. The bleaching time was 5.16 s and the total ROI fluorescence images after photobleaching were collected at intervals of 0.263 s at 512 × 512 pixel resolution using a pinhole of 600 μm, zoom factor 2.5 (with a zoom-in during bleaching) and 1000 Hz. Diffusion coefficients were calculated from FRAP experiments. Briefly, the mean fluorescence in the bleached region over time was converted to normalized fractional fluorescence intensity [3] according to the equation (1):

$$f = \frac{F_t - F_0}{F_\infty - F_0} \quad (1)$$

where $F_t$ is the fluorescence intensity at time t, $F_0$ is the fluorescence intensity immediately after bleaching, and $F_\infty$ is the fluorescence after complete recovery.

The normalized fractional fluorescence intensity was plotted versus time and fitted with an exponential curve. The fitting procedure was used to determine the half-recovery time τ at f = 0.5. Finally, the diffusion coefficient was calculated as by using the equation (2):

$$D = \frac{\omega^2}{4 * \tau} \quad (2)$$

where ω is the initial spot radius (40 μm).

For each FRAP measurement 5 bleach were performed on three independent experiments.

### 2.8. Immunofluorescence staining, imaging and quantification

10 μm thick slices for immunofluorescence staining, were obtained from formalin-fixed and paraffin embedded (FFPE) μTP and spheroids. Then, unmasking was obtained by heat antigen retrieval protocol by citrate buffer; then, sections were washed with PBS containing 0.2% Triton X-100, blocked with FBS and 5% BSA solution and incubated with primary antibody (E-cadherin 1:250, claudin-1 1:250, ZO-1 1:50, β-integrin 1:200 and P-gp 1:200). Alexafluor 596 was chosen as secondary antibody and DAPI staining was performed, before mounting the slices with glycerol solution. All the antibodies were purchased by Abcam (UK). To compare our results to a more realistic model, we stained FFPE slices of a mouse xenograft breast cancer model, kindly donated by Daidone's group. From spinner culture we collected equal amount of suspending media containing spheroids or μTP, which were then embedded in paraffin. 10 μm-thick slices for immunofluorescence staining, were obtained from formalin-fixed aggregates of spheroids or μTP; unmasking was obtained by heat antigen retrieval protocol by citrate buffer; then, sections were washed with PBS containing 0.2% Triton X-100, blocked with FBS and 5% BSA solution and incubated with primary antibody (E-cadherin 1:250, claudin-1 1:250, ZO-1 1:50, β-integrin 1:200 and P-gp 1:200). Alexafluor 596 was used as secondary antibody and DAPI staining was performed, before mounting the slices with glycerol solution. All the antibodies were obtained by Abcam (UK). To compare our results to a more realistic model, we stained FFPE slices of mouse xenograft breast cancer model, kindly donated by Daidone's group. Images were acquired by using multichannelled Leica TCS SP5 II, by applying the following setting at each acquisition: the planar size of the images was set at 1024 × 1024 pixels in order to have higher resolution; for DAPI/nuclei acquisition we used two photon mode configuration with laser intensity 10%, camera gain 5%, offset 42%; for the acquisition of Alexafluor596-labeled markers laser intensity was set at 40% and camera gain was set at 400. Then, by means of ImageJ we processed each image by using the equal levels of background subtrac-

tion (to remove noises) and threshold in each image. Moreover, after threshold, by using the resulting binary (black and white) images we counted the number of particles (in the case of cell nuclei) by using "Analyze particles" plugin, and the number of black pixel (in the case of proteins) by using "Measure" plugin. The measurement of both cell nuclei and proteins were performed in region of interests (ROI) contained in the tissue region of the μTP (Fig. S1), Such analyses were performed by two independent operators in order to reduce the uncertainty coming from the threshold. [30].

For immunofluorescence quantification were performed on 20 section of each sample and about 5 region of interests (ROI) were examined for each section acquired. Each experiment was repeated in triplicate.

### 2.9. Statistical analysis

Results were expressed as the mean ± s.e. (standard error) of n experiments. Statistical differences among the groups, were assessed by using a non parametric test such as Kruskal-Wallis. Statistical significance was considered at $p < 0.05$.

## 3. Results

### 3.1. In vitro imaging and cytotoxicity assay

Homotypic (MCF7) and heterotypic (CAF/MCF7) breast cancer models were fabricated as either microtissues or spheroids. All the obtained 3D models were exposed to DOX (at 4, 8 and 16 μg/ml) for 48 and 72 h to test DOX cytotoxic effect. In Fig. 1, we reported brightfield (Fig. 1A–D and I–N) and fluorescence (Fig. 1E–H and O–R) images of MCF7 spheroids and μTP after DOX treatment for 72 h. From spheroids brightfield images (Fig. 1A–D), a reduction of spheroid area was recorded, while no area reduction was detectable in μTP model (Fig. 1I–N). On the contrary, fluorescence images showed a higher DOX penetration in μTP model compared to spheroid model with the increase of DOX concentration (Fig. 1E–H and O–R). In both homotypic models, higher was the DOX concentration lower was the percent of cell viability (Fig. 1S–T). In particular, only after 72 h of DOX treatment a reduction of 50% of cell population has been reached for both models. In particular, the $IC_{50}$ (drug concentration to obtain the 50% of cell death) of DOX for MCF7 spheroids and μTP was calculated to be 8 μg/ml and 4 μg/ml, respectively (Fig. 1T). In Fig. 2, we reported optical (Fig. 2A–D and I–N) and fluorescence (Fig. 2E–H and O–R) images of heterotypic spheroids and μTP after DOX treatment for 72 h. Brightfield images of spheroids (Fig. 2A–D) indicated that the effect of DOX was strictly limited to the outer cell layers (dead cells detached from the spheroid configuration) but the spheroid area remained roughly the same. On the other hand, the size of heterotypic μTP treated with DOX (Fig. 2I–N) was reduced with the extending of exposure time and the increase of drug concentration. The effect was prominent when treated with DOX at concentration of 16 μg/ml for 72 h. Furthermore, drug penetration and distribution were assessed by confocal microscopy observations. Confocal images (Fig. 2E–H and O–R) showed that DOX penetration was higher at 72 h than 48 h for both models. After 72 h of treatment, DOX penetrated into the nuclei of 3D cultured cells in a dose-dependent manner. Especially, DOX displayed a homogeneous and dose-dependent accumulation region in μTP. After 72 h, DOX penetration was higher in μTP (Fig. 2O–R) than spheroids (Fig. 2F–H) suggesting that μTP structure was less compact than spheroids and thus more readily allows the penetration of drugs at very high concentrations. Furthermore, SHG signal (Fig. 2O–R, in gray scale) was detected only in μTP configuration, indicating the presence of collagen fibers produced and assembled by fibroblasts. SHG images showed a random distribution of fiber orientations and a wide inter-fiber spacing in tumors. In order to verify that the SHG signal observed in the μTP was related to an endogenous production of collagen, an image of the gelatin porous microbeads before the complete degradation in a microtissues is reported (Fig. S1). As shown in the Fig. S1, the gelatin provided a different SHG signal that cannot be related to the collagen signal produced by the cells in the microtissues. MTT cytotoxicity results shown in Fig. 2S and T, reveals that there was no inhibition effect in cell proliferation after the treatment of CAF/MCF7-sph with DOX both at 48 and 72 h. On the contrary, the $IC_{50}$ in CAF/MCF7-μTP is observed at 8 μg/ml of DOX exposure for 72 h. However, the inhibition of cell viability for CAF/MCF7-μTP was lower than that the homotypic μTP counterparts. Definitely, MTT results demonstrated that heterotypic cultures with stromal fibroblasts exhibit significantly higher drug resistance than homotypic cultures both in spheroid and μTP model. These results highlighted the importance of having a multicellular model to replicate the interaction between cancer and stromal cells, such as fibroblasts as in this case. Moreover, we observed that, beside multi-cellularity, the presence of a cell-assembled ECM in the μTP model also played a crucial role in modulating the drug response.

### 3.2. Molecular transport in μTP and spheroid

To better understand the difference in DOX transport in two models, we have focused on diffusion coefficient through the interstitial space of spheroids and μTP. We measured the diffusion coefficient of fluorescein in homotypic (MCF7-) and heterotypic (CAF/MCF7-) spheroids and μTP using FRAP, which measures the fluorescent intensity recovery in the bleached region over time (Fig. 3E). The measured diffusivity within μTP was 3.95 ± 0.70 E-07 $cm^2/s$ and 2.10 ± 0.54 E-07 $cm^2/s$ for MCF7- and CAF/MCF7-μTP, respectively. In spheroid model, the diffusion coefficient is equal to 1.98 ± 0.48 E-07 $cm^2/s$ for MCF7 and 1.27 ± 0.45 E-07 $cm^2/s$ for CAF/MCF7 culture. In both cases, the diffusion coefficient decreased with the complexity of the system from homotypic to heterotypic culture but increased in μTP configuration respect to spheroid model. Finally, spheroids showed lower diffusion coefficient of the molecular probe having molecular weight similar to the DOX compared to μTP (Fig. 3E).

### 3.3. Expression of cell adhesion molecules in μTP and spheroid models

Since adhesion molecules play an important role in cell morphology and function, we investigated whether the expression of E-cadherin, ZO-1 and Claudin-1 differed in homotypic and heterotypic conditions in spheroids and μTP. Fig. 4 shows fluorescence images of cell adhesion marker E-cadherin (in red) in MCF7-sph (Fig. 4A), CAF/MCF7-sph (Fig. 4C), MCF7-μTP (Fig. 4B), CAF/MCF7-μTP (Fig. 4D), and in the mouse xenograft slice (Fig. 4E), respectively. Quantification analysis (Fig. 4F) revealed a higher E-cadherin expression level in the case of spheroids, both homotypic and heterotypic respect to μTP counterparts and xenograft model ($p < 0.05$). The same trend was found for claudin-1 (Fig. 5A–E) and ZO-1 (Fig. 6A–E) expressions in spheroids and μTP. In particular, the level of ZO-1 expression is equal between MCF7 spheroids and μTP (Fig. 6F) ($p > 0.05$) but it was shown the loss of these tight junctions when MCF7 were cultured with CAF in heterotypic μTP. These results showed that the expression of adhesion and tight molecules in μTP model was more similar to that of tumors grown *in vivo* than those of spheroid-cultured cells.

Fig. 7A–E show fluorescence images of cell adhesion markers β1-integrin (in red) in homotypic and heterotypic spheroids and μTP, respectively. From quantification analysis we found a slight

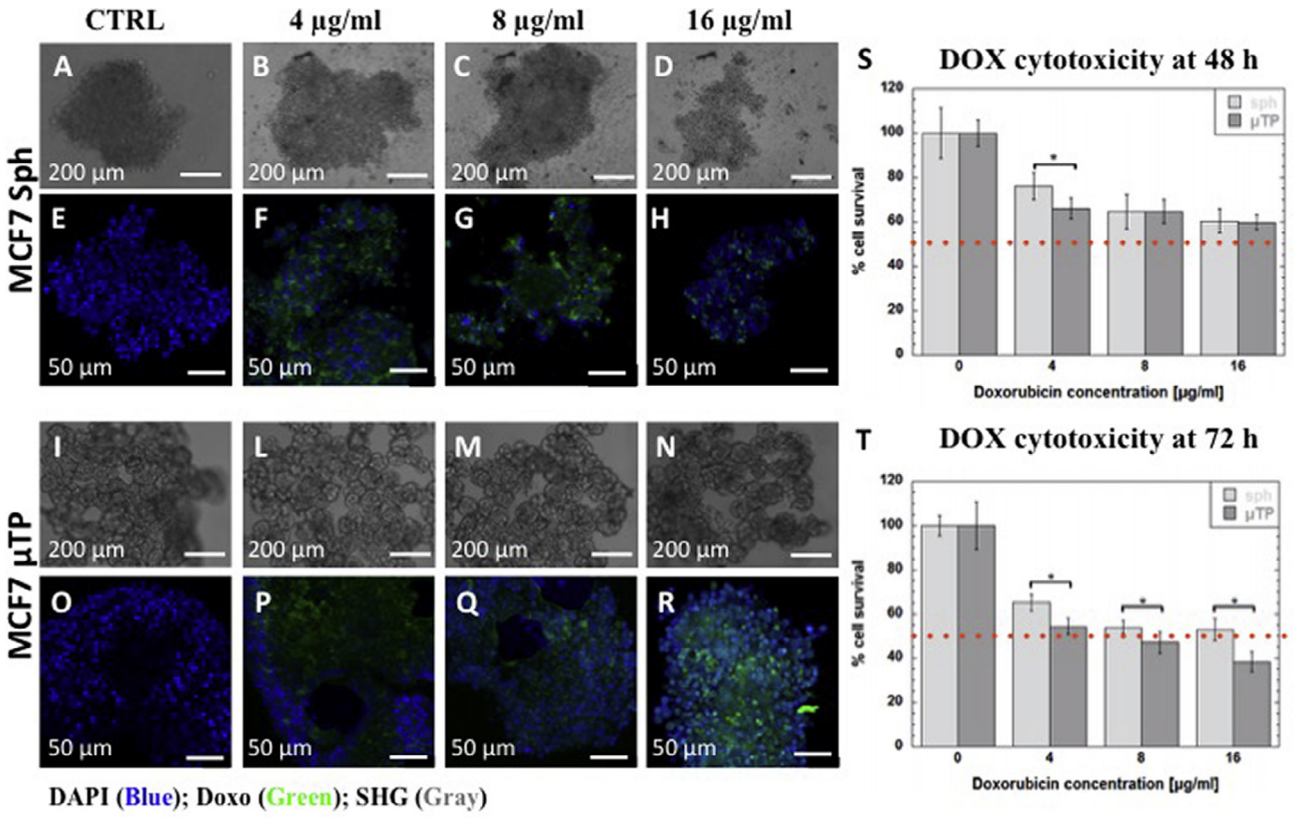


**Fig. 1.** Brightfield images of MCF7-sph (A–D) and MCF7-µTP (I–N) after 72 h of DOX treatment at 4, 8 and 16 µg/ml (A, I controls), scale bar 100 µm. Fluorescence distribution of DOX within MCF7-sph (E–H) and MCF7-µTP (O–R) upon 72 h incubation with DOX at 4, 8 and 16 µg/ml (E, O controls), scale bar 50 µm. Cytotoxicity assay in MCF7-sph (light gray) and MCF7-µTP (middle gray) after treatment with DOX at 4, 8 and 16 µg/ml for 48 (S) and 72 h (T).

higher expression level in the case of spheroids, both homotypic (Fig. 7A) and heterotypic (Fig. 7C) respect to µTP counterparts (Fig. 7B and D) and xenograft model (Fig. 7E) ($p < 0.05$). We also analyzed the expression of P-gp protein (Fig. 8A–E) in the different 3D tumor models and in xenograft slices, by mean of immunofluorescence. We found that cells in µTP conformation express higher level of P-gp compared to spheroids. On the other hand, P-gp expression level in µTP are similar to the xenograft one (Fig. 8F).

## 4. Discussions

In the present study, the effect of DOX on cell proliferation, drug penetration and diffusion as well as the expression of proteins related to cell-cell and cell-ECM junctions and chemoresistance, was investigated in two different 3D breast cancer models, namely microtissues and spheroids, where breast cancer cells were grown in monoculture or in coculture with cancer associated fibroblasts. It is well known that tumor *in vivo* is not merely an aggregation of cancer cells but a complex entity in which cancer cells interplay with stroma cells and ECM and together contribute to the mechanism leading to drug resistance [31,32]. The cellular components of TME interact with tumor cells and impact various biological characteristics such as proliferation, migration and therapeutic resistance [33]. The non-cellular components of TME play an equally significant role in cancer progression, by presenting cues that affect fundamental aspects of tumor cell biology [5,34]. It becomes important to incorporate both the cellular and acellular components of tumor stroma in 3D models to obtain a more realistic drug screening tool [35]. Typically, the golden standard for *in vitro* tumors recapitulation is the spheroid since it exhibits many of the biological properties of solid tumors, including cell morphology, growth kinetics and gene expression. Spheroid results very useful, with respect to 2D culture, to gain insight into therapeutic problems associated with metabolic and proliferative gradients, such as the altered responsiveness and effects of chronically hypoxic tumor cells, and the importance of increased cell-cell contacts, in radio and chemo-resistance. Spheroids cannot, however, recapitulate all features of solid tumors possessing a strong desmoplastic reaction, since they lack the interactions with the ECM that plays a key-role in tumor progression and chemoresistance. It is generally accepted that diffusion gradients exist within spheroids for oxygen and nutrients, and that the availability of these compounds to the innermost cells is limited. It is therefore likely that the diffusion of most drugs, which are typically much larger than oxygen and carbon dioxide molecules, will be limited within spheroids as well. The results of this work demonstrated that CAF/MCF7-µTP better resembles the tumor microarchitecture than spheroids, because the presence of the microcarriers allows fibroblasts to synthesize collagen and sustains its assembly reproducing the tumor architecture found *in vivo* [34]. In both models, the coculture of cancer cells with fibroblasts not only elicits physicochemical changes of cancer cells and microenvironment, but also brings about differences in drug response compared to single culture of cancer cells [36,37]. Furthermore MCF7-sph model results less responsive to DOX respect to µTP configuration. The possible reasons can be conferred to the spheroid tight morphology that blocks the diffusion of drug to the outer layers in which cells are more proliferative and therefore more sensible to DOX treatment. It has already known that some of the traditionally administered chemotherapic drugs have high proliferative cells as targets. However this cells develop resistance to anti-cancer drugs, that if from

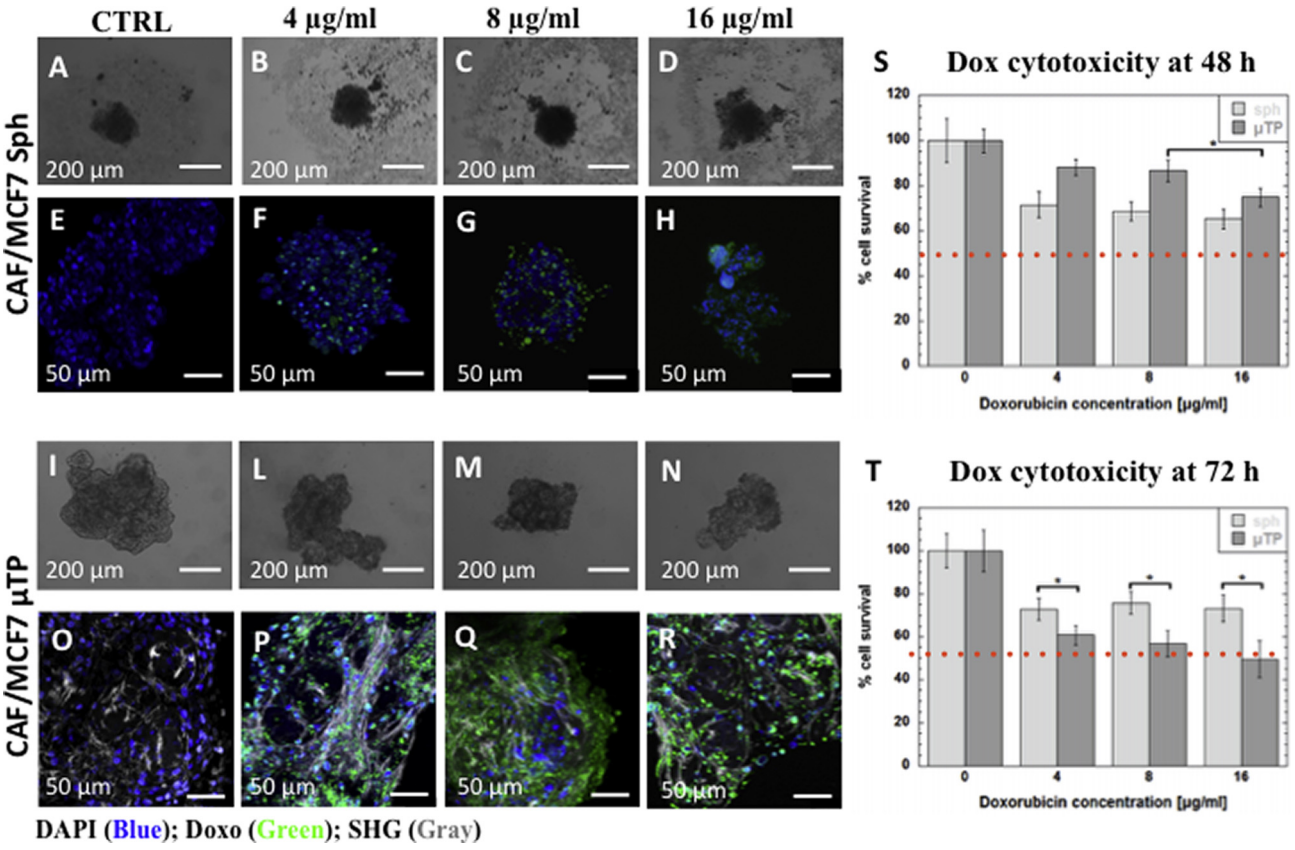


**Fig. 2.** Brightfield images of CAF/MCF7-sph (A–D) and CAF/MCF7-µTP (I–N) after 72 h of DOX treatment at 4, 8 and 16 µg/ml (A, I controls), scale bar 100 µm. Fluorescence distribution of DOX within CAF/MCF7-sph (E–H) and CAF/MCF7-µTP (O–R) upon 72 h incubation with DOX at 4, 8 and 16 µg/ml (E, O controls), scale bar 50 µm. Cytotoxicity assay in CAF/MCF7-sph (light gray) and CAF/MCF7-µTP (middle gray) after treatment with DOX at 4, 8 and 16 µg/ml for 48 (S) and 72 h (T). SHG signal has been detected only in CAF/MCF7-µTP, showing a greater potential for the microcarriers based tumor model.

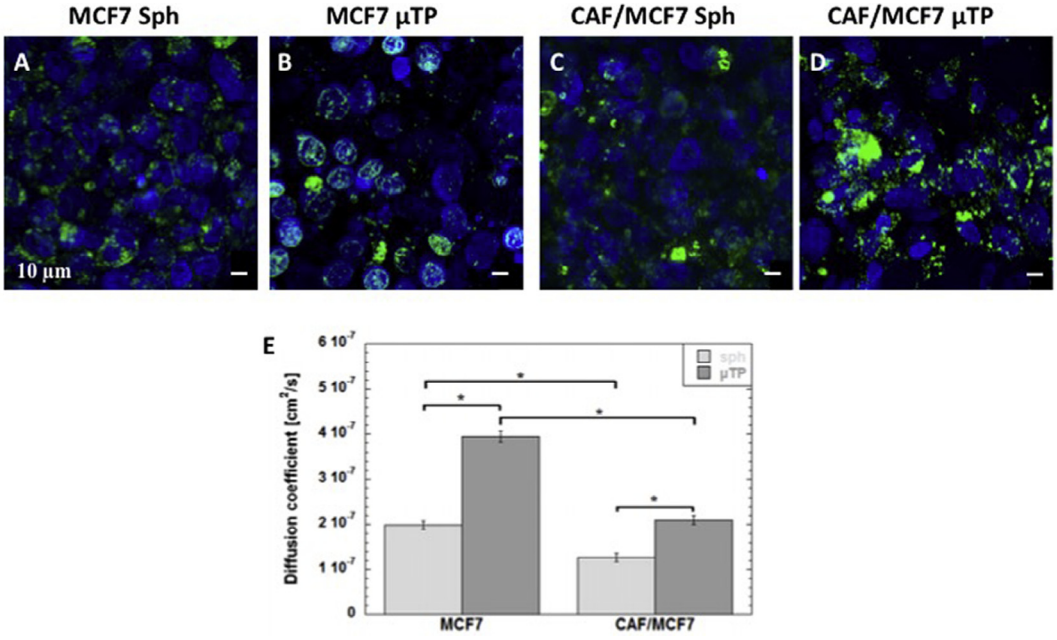


**Fig. 3.** Fluorescence images of DOX within MCF7-sph (A) and MCF7-µTP (B) and within CAF/MCF7-sph (C) and CAF/MCF7-µTP (D) at high magnification after 72 h incubation with DOX at 8 µg/ml, scale bar 10 µm; Diffusion coefficients (D) of Fluorescein in MCF7- and CAF/MCF7-sph (light gray) and MCF7- and CAF/MCF7-µTP (middle gray).

one side are able to internalize the drug, on the other they over-express efflux pump proteins that make the cells resistant to the treatment, flushing out drugs [38]. Nevertheless, monoculture models show some limits because of the lack of stromal component, so they do not represent the ideal drug screening platform. Beside the presence of ECM that plays a relevant role in drug

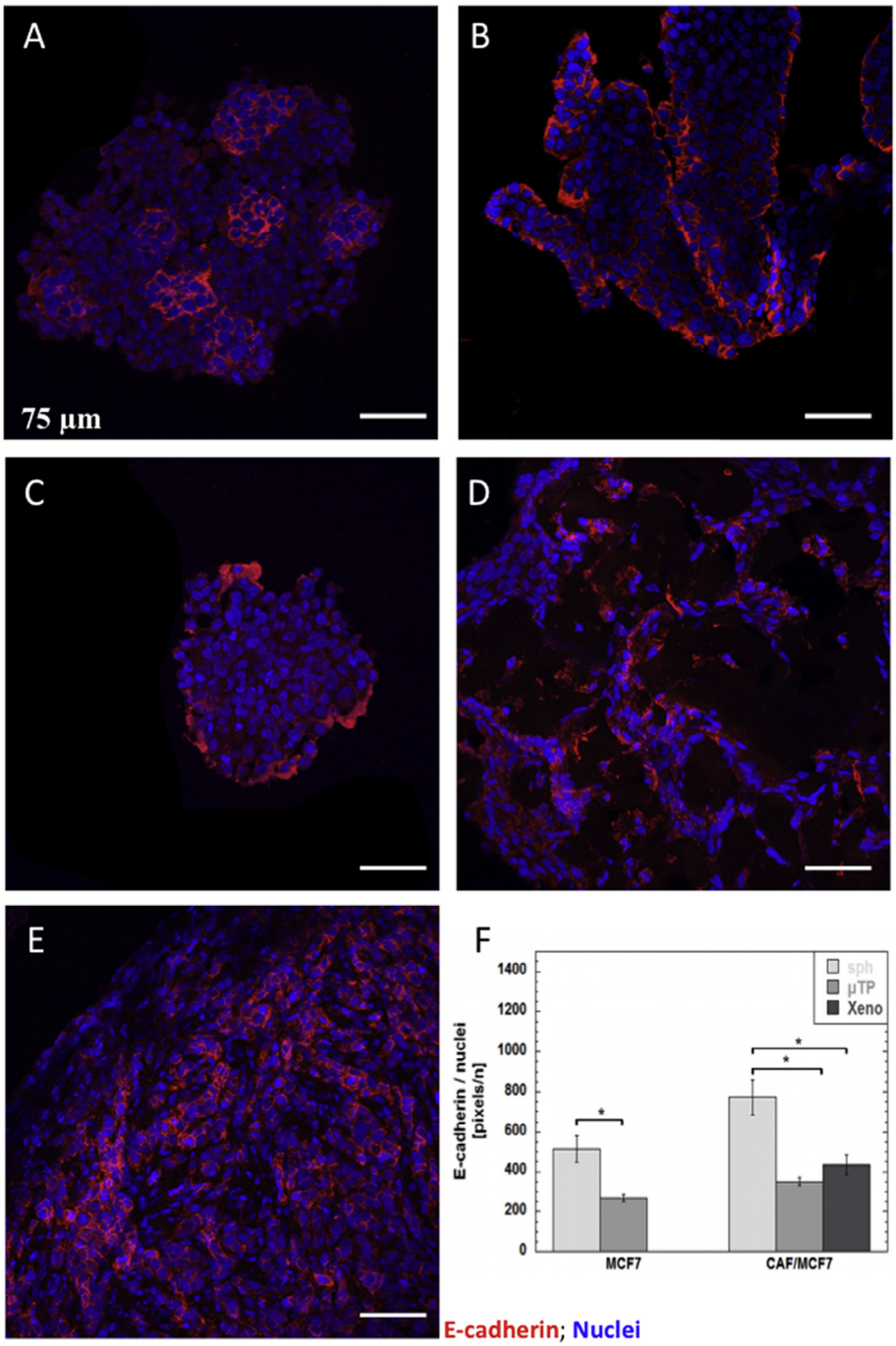


**Fig. 4.** E-cadherin fluorescence images (red signal) in MCF7-sph (A), MCF7-µTP (B), CAF/MCF7-sph (C), CAF/MCF7-µTP (D) and in xenograft mouse model (E). Quantification of E-cadherin (F) expression (pixels/nuclei) in MCF7-sph, MCF7-µTP, CAF/MCF7-sph, CAF/MCF7-µTP and in xenograft mouse model. Asterisks indicate statistical differences with $p < 0.05$. (For interpretation of the references to colour in this figure legend, the reader is referred to the web version of this article.)

diffusion, we hypothesizes that cancer associated fibroblasts also give a different response to DOX, since co-culture of both spheroids and µTP, were less responsive to DOX. A difference in cell proliferation rate or in the mechanism for DNA repair (impaired by DOX) between fibroblast and cancer cells could also be a reason for a different behavior of mono-culture and co-culture in response to DOX. A previous mathematical model has predicted that drug penetration is the most crucial factor in determining drug effectiveness in spheroids [39]. When we cultured MCF7 with CAF, drug mass transfer was expected to be much more limited respect to monoculture due to stromal barrier. Recently, a work has demonstrated that hetero-spheroid conditions with stromal fibroblasts exhibit enhanced resistance to drug over homospheroids [13]. This finding is confirmed also in our study, where the CAF/MCF7 co-culture configuration both for spheroid or microtissues exhibited a significant resistance to DOX. In particular, drug concentration in CAF/MCF7-sph increased over time but it was not sufficient to achieve the $IC_{50}$ value. Meanwhile, CAF/MCF7-µTP halved their viability after DOX treatment with a concentration of 8 µg/ml. This difference could be explained by the different morphology of the two analyzed 3D tumor models. In fact, in spheroids, DOX kills the cells in active proliferation on the outer region, reducing their diameter while in the µTP models the DOX penetrates in the inner part of the tumor, killing a larger amount of cells, but, due to the

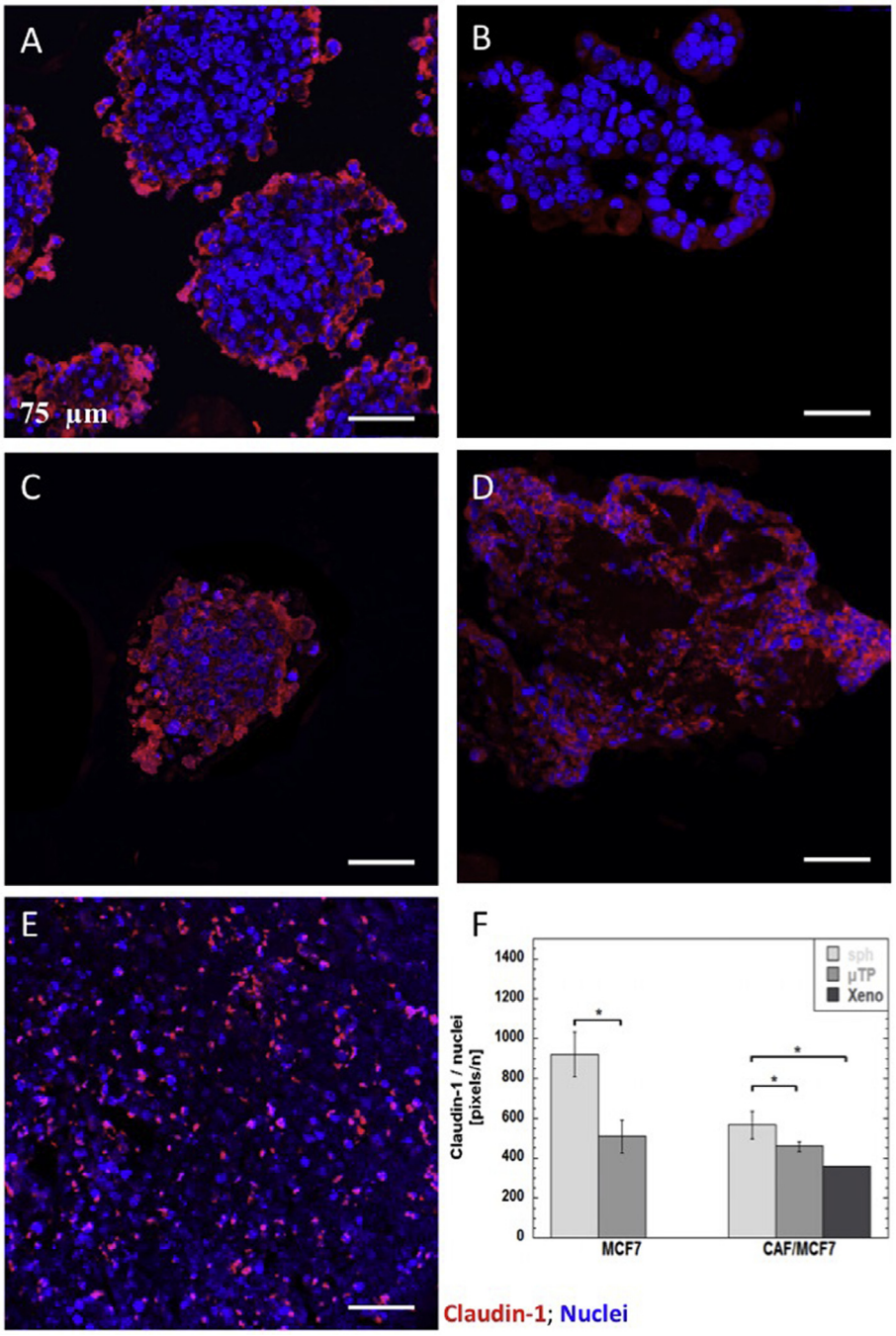


**Fig. 5.** Claudin-1 fluorescence images (red signal) in MCF7-sph (A), MCF7-µTP (B), CAF/MCF7-sph (C), CAF/MCF7-µTP (D) and in xenograft mouse model (E). Quantification of Claudin-1 (F) expression (pixels/nuclei) in MCF7-sph, MCF7-µTP, CAF/MCF7-sph, CAF/MCF7-µTP and in xenograft mouse model. Asterisks indicate statistical differences with $p < 0.05$. (For interpretation of the references to colour in this figure legend, the reader is referred to the web version of this article.)

presence of a dense structured ECM, the size of the µTP is poorly affected in the short period. Moreover, the different behavior can be attributed to different morphology of models, so it could be hypothesized that the rapid drug penetration in µTP might be possible due to the greater intercellular space between cells. Therefore, it may be argued that the aforementioned findings are attributable to a diminished drug diffusion coefficient in spheroids as demonstrated by FRAP experiments [40]. Previous studies using fluorescent drugs or macromolecules have been shown poor penetration of DOX into deeper layers of spheroids [41]. However, it was demonstrated that drugs (such as anthracyclines) accumulated preferentially in cells at the periphery of spheroids, reducing drug cytotoxic activity [42]. These data strongly confirmed the results obtained in our work in terms of drug penetration in spheroid model. The difference of the cellular distribution of DOX in spheroids and µTP suggested that there are different physical barriers that hinder the diffusion of drugs. In our work, we demonstrated the presence of cell-synthesized collagen fibers in CAF/MCF7-µTP, but not in CAF/MCF7-sph. Although matrix components could be considered a barrier to drug transport, the rapid ECM turnover due to the proteases secreted by the cancer cells, as we also stated in our previous work [23] in µTP model allowed more drugs to infiltrate more freely inside the matrix structure, increasing DOX anti-cancer activity. One of the key features of epithelial

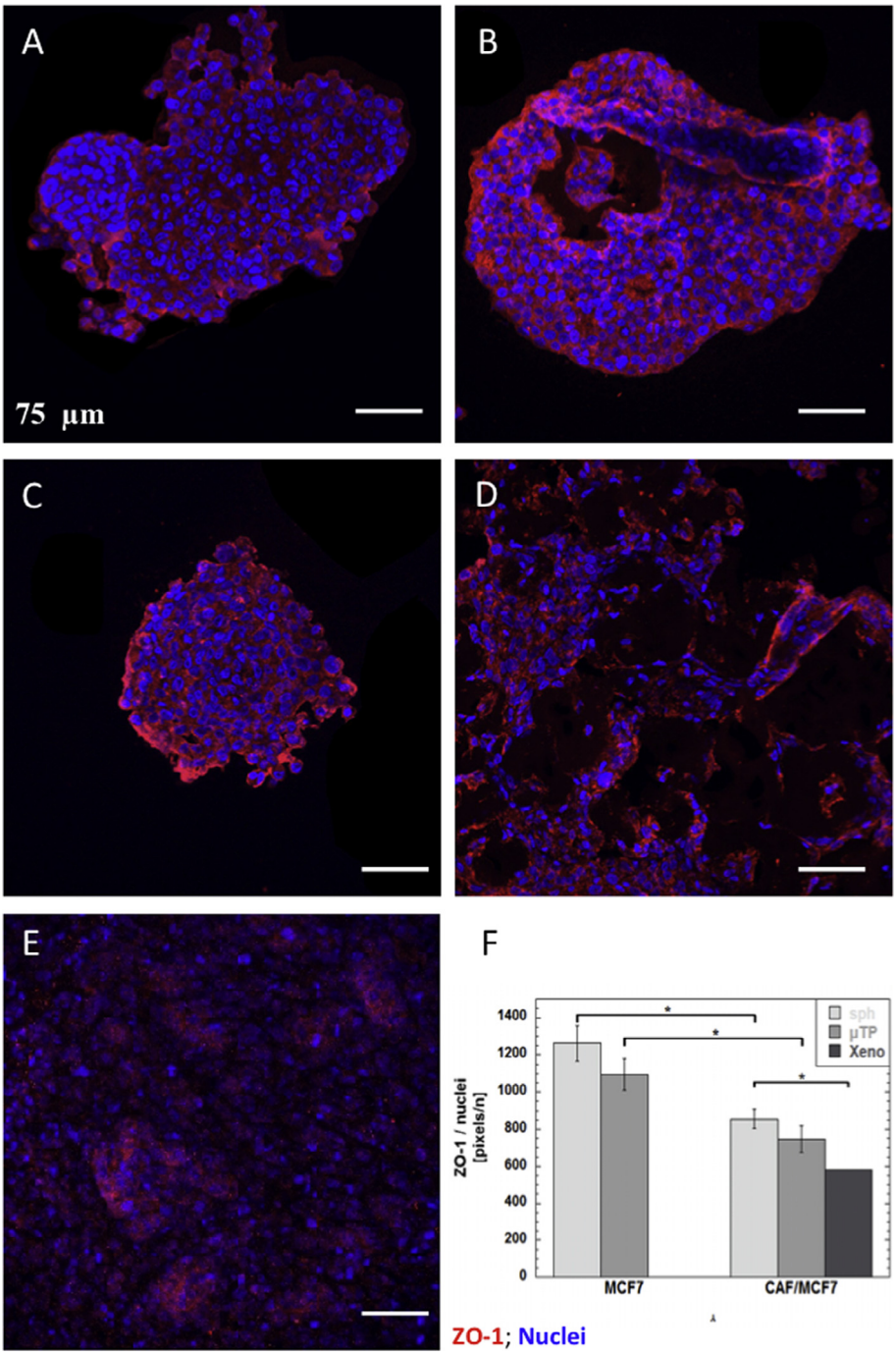


**Fig. 6.** ZO-1 fluorescence images (red signal) in MCF7-sph (A), MCF7-µTP (B), CAF/MCF7-sph (C), CAF/MCF7-µTP (D) and in xenograft mouse model (E). Quantification of ZO-1 (F) expression (pixels/nuclei) in MCF7-sph, MCF7-µTP, CAF/MCF7-sph, CAF/MCF7-µTP and in xenograft mouse model. Asterisks indicate statistical differences with $p < 0.05$. (For interpretation of the references to colour in this figure legend, the reader is referred to the web version of this article.)

tumors is the presence of intercellular junctions, which link cells to one another, and act as barriers to the penetration of molecules with a molecular weight greater than 400 Da, as DOX. Furthermore, intercellular contacts promote cell survival through activation of signaling pathways such as PI3K/Akt, NF-kB and Stat3 [35]. In particular, in most solid tumors derived from epithelial tissues presents nests of malignant tumor cells are linked through junction proteins such as E-cadherin, claudins and ZO-1 [43]. Previous studies using multicellular layer models have shown poor drug distribution into tumors with high packing density [40]. In our case, impaired penetration of anticancer agents through spheroids, both homotypic and heterotypic, derived from cells with tightly packed cells in comparison with loose packing cells in µTP model. In this work we further examined one of the most important adhesion junctions, the E-cadherin, in both models. E-cadherin is thought to function as a tumor suppressor in numerous tissues and has been shown to be a useful prognostic indicator for some tumors [44]. As reported in recent papers, the presence of strong cell-cell adhesion mediated by E-cadherin prevent cell apoptosis and therefore promote cell survival [44]. In this way, when CAF/MCF7-sph were exposed to DOX treatment, were more resistant to drug due to high cell-cell adhesions. On the contrary,

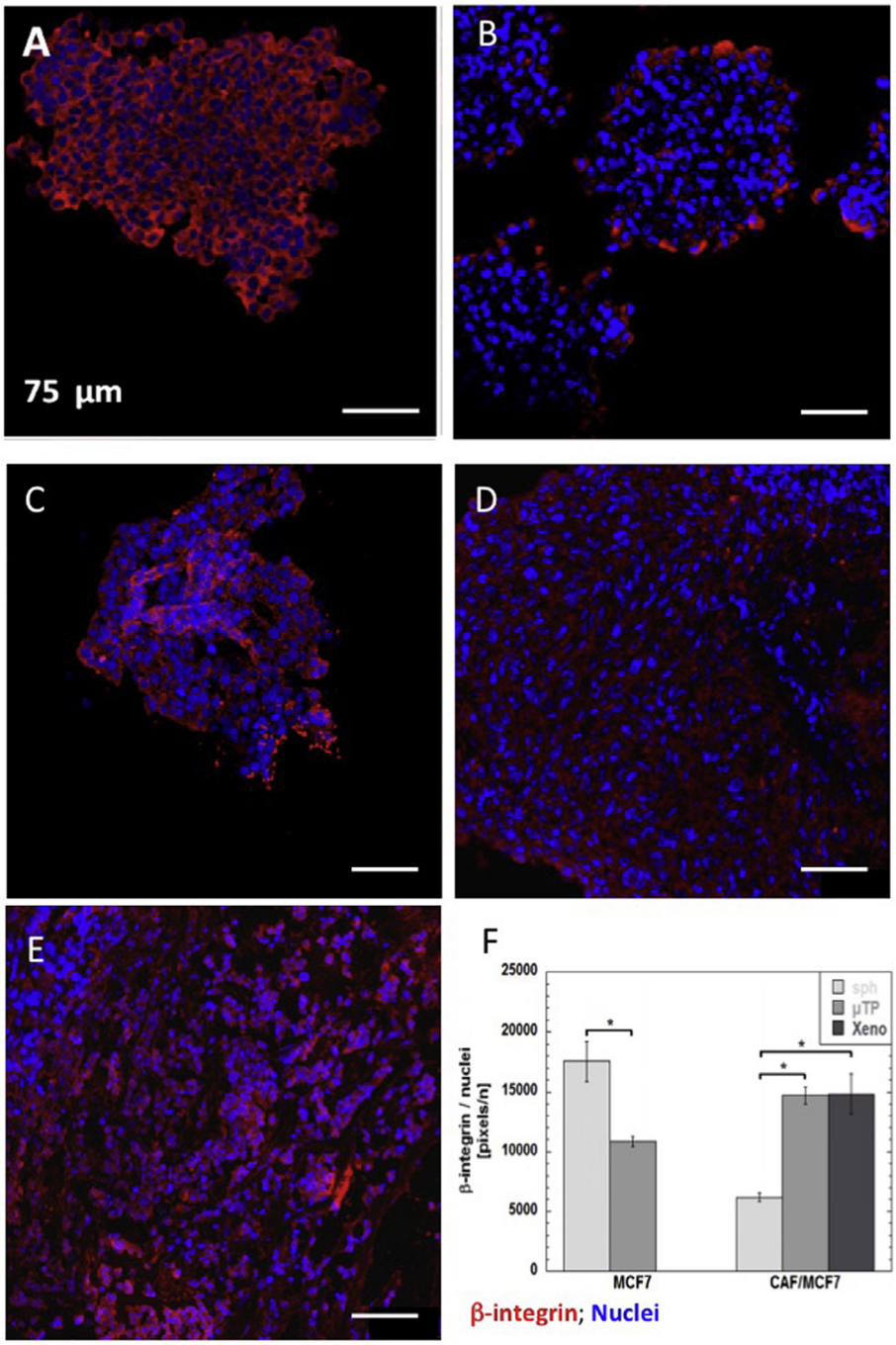


**Fig. 7.** β-integrin fluorescence images (red signal) in MCF7-sph (A), MCF7-µTP (B), CAF/MCF7-sph (C), CAF/MCF7-µTP (D) and in xenograft mouse model (E). Quantification of β-integrin (F) expression (pixels/nuclei) in MCF7-sph, MCF7-µTP, CAF/MCF7-sph, CAF/MCF7-µTP and in xenograft mouse model. Asterisks indicate statistical differences with $p < 0.05$. (For interpretation of the references to colour in this figure legend, the reader is referred to the web version of this article.)

in CAF/MCF7-µTP exhibited lower expression of epithelial cell adhesion markers E-cadherin. One of the important role of tight junctions is the permeability barrier function that regulates the passage of water, ions and various macromolecules through intercellular spaces [45]. Tokes et al. (2005), have demonstrated a significant loss of claudin-1 protein in breast cancer cells in sections from surgically resected breast specimens by immunostaining [46]. In our work, we reported a loss of claudin-1 and ZO-1 proteins in CAF/MCF7-µTP, showing a quite similar situation in xenograft model. These results are in accordance with previous works in human tumors where levels of ZO-1 were significantly lower in patients with metastatic disease compared with those remaining disease-free [47]. Along the analysis for the protein involved in tight junction, we found a proof of evidence that the 3D tumor models presented in this paper, express β1-integrin on the surface of the cells. Moreover integrins are involved in cellular processes, such as cell anchorage, migration, differentiation and death, where they represent a bridge between ECM and actin cytoskeleton. In cancer they are over expressed, indicating poor prognosis for the patients [48]. It has already been demonstrated that integrins showed a different expression profile when they are analyzed in 2D or 3D condition [49–51], furthermore there are some differences in expression when cells are arranged in quite different 3D tumor models as we demonstrate in the present survey. It is

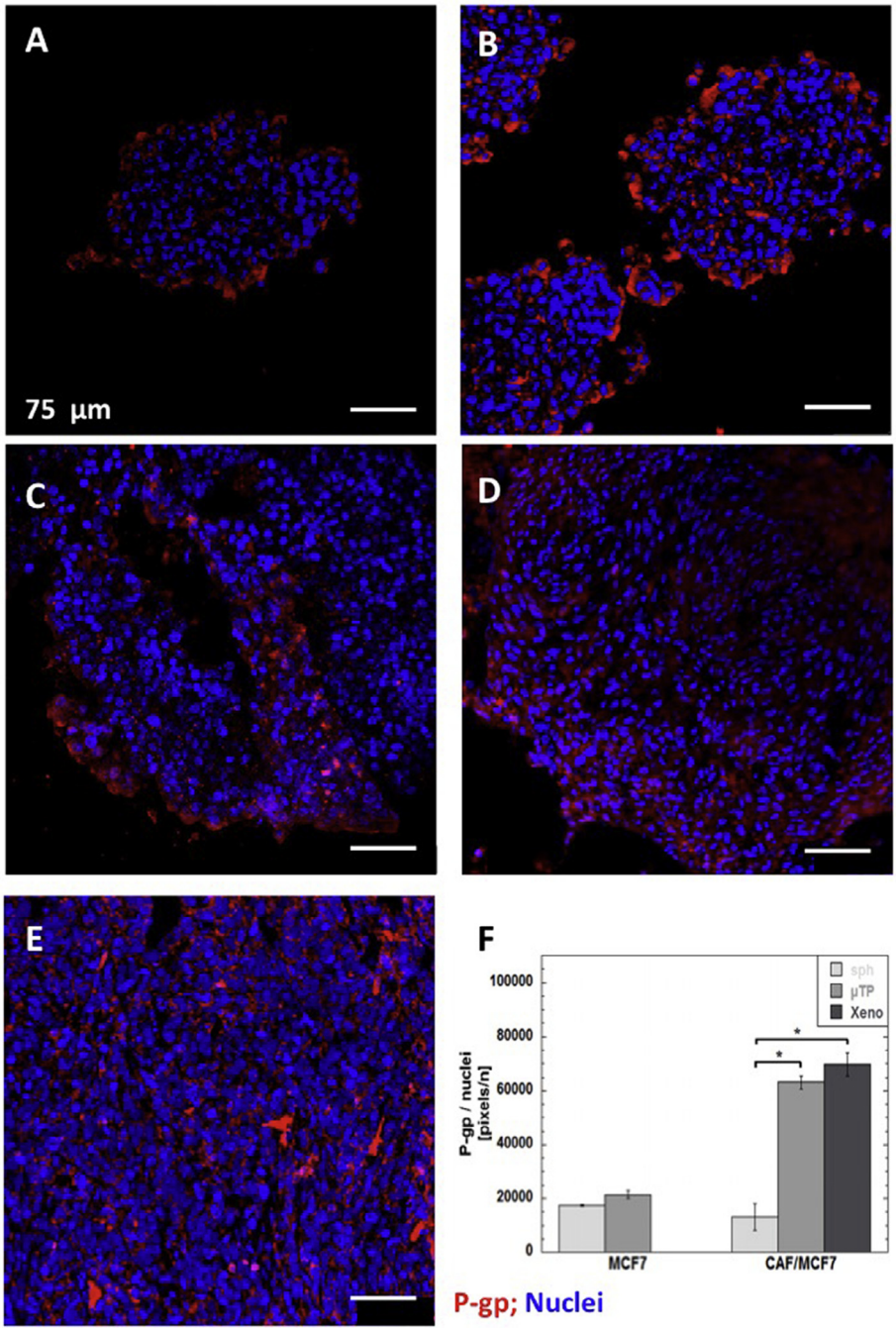


**Fig. 8.** P-gp fluorescence images (red signal) in MCF7-sph (A), MCF7-µTP (B), CAF/MCF7-sph (C), CAF/MCF7-µTP (D) and in xenograft mouse model (E). Quantification of P-gp (F) expression (pixels/nuclei) in MCF7-sph, MCF7-µTP, CAF/MCF7-sph, CAF/MCF7-µTP and in xenograft mouse model. Asterisks indicate statistical differences with $p < 0.05$. (For interpretation of the references to colour in this figure legend, the reader is referred to the web version of this article.)

already known that resistance to chemotherapic drugs is correlated to the overexpression of multidrug resistance (MDR) 1P-glycoprotein (P-gp), a glycosylated *M*r 170,000. P-gp is an efflux pump that has the task to expel toxins in physiological conditions. In cancer, it is likelihood associated to treatment failure [52]. P-gp can bind a large variety of hydrophobic natural-product drugs, included doxorubicin. It has already been demonstrated that multicellular spheroids show a higher resistance to anticancer drugs when compared to monolayer culture, highlighting the importance to have a multicellular tissue architecture in 3D dimension [53]. The produced breast cancer microtissues could be defined a complex biological system in which cells embedded in their own ECM are able to experience physiological cell-cell and cell-ECM interactions. The endogenous ECM surrounding the cells could exert the repository and regulatory role of the microenvironment in tumor development. Spheroid could be embedded in different type of ECM, but the added ECM surrogates are of exogenous origin and not produced by the cells during the tumor model build-up. In our model, stromal cells are engaged in a continuous remodeling and turnover of their own ECM. We have previously demonstrated that exogenous ECMs, although biocompatible, are not able to displays the architectural and compositional changes during the progression of pathologic status [19,54]. In other words: healthy fibroblast synthesize healthy stroma; pathologic fibroblast

synthesize pathologic stroma; if one stars from an healthy status and then a transition toward pathologic one is induced, both fibroblasts and their own ECM evolve toward the pathologic status [19,54]. Such ECM responsiveness is not replicated in exogenous ECMs, we believe that this is a uniqueness of the systems in which cells build-up their extracellular space. For this reason we argue that our tumor microtissues could represent an innovative tool for the characterization of disease progression and drug response *in vitro*. Moreover due to their size at a sub-millimetric scale, they could be easily inserted in miniaturized fluidic devices for tissue-on-chip applications. In this paper we demonstrate that there is a better similarity between xenograft and 3D microtissues when we analyze the presence of some membrane proteins involved in cell-cell or cell-ECM junctions, or multidrug resistance pathway. Xenografts, on the other hand, involve the use of animals lowering the predictability of the tests. In this perspective we conjecture that μTP is a superior model to study those aspects of cancer progression related the ECM dynamics [30,31], compared to the spheroids.

## 5. Conclusions

In this study, we report a 3D *in vitro* cancer model that can be used for the investigation of drug response against breast cancer cells. Our system has presented several advantages respect to the classical spheroid model: the biodegradable microscaffolds have a good porosity that provide the spatial interconnectivity between cells and affect the synthesis of endogenous ECM by stromal cells. Moreover tumor cells have lower expression of adhesion molecules, typical aspect observed during tumorigenesis. Since the morphology of our system is closer to *in vivo* model, when compared to the spheroid model observed, it suggests that the μTP system may be a useful *in vitro* model to study the efficacy of drugs that also affect the tumor microenvironment.

## Disclosure

The authors report no conflicts of interest in this work.

## Acknowledgements

We would like to thank: Dr. Valentina La Tilla for her graphical support; Dr. Martina Profeta for her technical support; the group of Maria Grazia Daidone, IRCCS Istituto Nazionale Tumori Via Venezian 1 20133 Milano for providing mouse xenograft breast cancer model. Moreover, we are grateful for financial support provided by the following grants: FIRB project Newton (RBAP11BYNP_004) of the Italian Ministry of Education, University and Research (MIUR).

## Appendix A. Supplementary data

Supplementary data associated with this article can be found, in the online version, at https://doi.org/10.1016/j.actbio.2018.05.055.

## References

[1] S. Nath, G.R. Devi, Three-dimensional culture systems in cancer research: Focus on tumor spheroid model, Pharmacol. Ther. 163 (2016) 94–108.
[2] J.L. Horning, S.K. Sahoo, S. Vijayaraghavalu, S. Dimitrijevic, J.K. Vasir, T.K. Jain, A.K. Panda, V. Labhasetwar, 3-D tumor model for *in vitro* evaluation of anticancer drugs, Mol. Pharm. 5 (2008) 849–862.
[3] A. Villasante, G. Vunjak-Novakovic, Tissue-engineered models of human tumors for cancer research, Expert Opin. Drug Discov. 10 (2015) 257–268.
[4] L.W. Dunne, Z. Huang, W. Meng, X. Fan, N. Zhang, Q. Zhang, Z. An, Human decellularized adipose tissue scaffold as a model for breast cancer cell growth and drug treatments, Biomaterials 35 (2014) 4940–4949.
[5] X. Zhang, W. Wang, W. Yu, Y. Xie, X. Zhang, Y. Zhang, X. Ma, Development of an in vitro multicellular tumor spheroid model using microencapsulation and its application in anticancer drug screening and testing, Biotechnol. Prog. 21 (2005) 1289–1296.
[6] M.R. Carvalho, D. Lima, R.L. Reis, V.M. Correlo, J.M. Oliveira, Evaluating biomaterial- and microfluidic-based 3D tumor models, Trends Biotechnol. 33 (2015) 667–678.
[7] V.B.L. Weiswald, D. Bellet, Spherical cancer model in tumor biology, Neoplasia 17 (2015) 1–15.
[8] M. Lal-Nag, L. McGee, R. Guha, E. Lengye, H.A. Kenny, M. Ferrer, A high-throughput screening model of the tumor microenvironment for ovarian cancer cell growth, SLAS Discov. 22 (2017) 494–506.
[9] D.V. LaBarbera, B.G. Reid, B.H. Yoo, The multicellular tumor spheroid model for high-throughput cancer drug discovery, Expert Opin. Drug Discov. 7 (2012) 819–830.
[10] S. Ong, Z. Zhao, T. Arooz, D. Zhao, S. Zhang, T. Du, M. Wasser, D. van Noort, H. Yu, Engineering a scaffold-free 3D tumor model for *in vitro* drug penetration studies, Biomaterials 31 (2010) 1180–1190.
[11] W.J. Ho, E.A. Pham, J.W. Kim, C.W. Ng, J.H. Kim, D.T. Kamei, B.M. Wu, Incorporation of multicellular spheroids into 3-d polymeric scaffolds provides an improved tumor model for screening anticancer drugs, Science 101 (2010) 2637–2643.
[12] D. Loessner, K.S. Stok, M.P. Lutolf, D.W. Hutmacher, J.A. Clements, S.C. Rizzi, Bioengineered 3D platform to explore cell-ECM interactions and drug resistance of epithelial ovarian cancer cells, Biomaterials 31 (2010) 8494–8506.
[13] D. Yip, C.H. Cho, A multicellular 3D heterospheroid model of liver tumor and stromal cells in collagen gel for anti-cancer drug testing, Biochem. Biophys. Res. Commun. 433 (2013) 327–332.
[14] S. Krueger, T. Kalinski, H. Wolf, U. Kellner, A. Roessner, Interactions between human colon carcinoma cells, fibroblasts and monocytic cells in coculture-regulation of cathepsin B expression and invasiveness, Cancer Lett. 223 (2005) 313–322.
[15] L.A. Kunz-Schughart, P. Heyder, J. Schroeder, R. Knuechel, A heterologous 3-D coculture model of breast tumor cells and fibroblasts to study tumor-associated fibroblast differentiation, Exp. Cell Res. 266 (2001) 74–86.
[16] E.C. Costa, A.F. Moreira, D. de Melo-Diogo, V.M. Gaspar, M.P. Carvalho, I.J. Correia, 3D tumor spheroids: an overview on the tools and techniques used for their analysis, Biotechnol. Adv. 34 (2016) 1427–1441.
[17] N. Baek, O.W. Seo, M. Kim, J. Hulme, S.S. An, Monitoring the effects of doxorubicin on 3D-spheroid tumor cells in real-time, Oncol. Tragets Ther. 22 (2016) 7207–7218.
[18] W. Zhang, C. Li, B.C. Baguley, F. Zhou, W. Zhou, J.P. Shaw, Z. Wang, Z. Wu, J. Liu, Optimization of the formation of embedded multicellular spheroids of MCF-7 cells: How to reliably produce a biomimetic 3D model, Anal. Biochem. 515 (2016) 47–54.
[19] V. Brancato, A. Garziano, F. Gioiella, F. Urciuolo, G. Imparato, V. Panzetta, S. Fusco, P. Netti, 3D is not enough: building up a cell instructive microenvironment for tumoral stroma microtissues, Acta Bomater. 47 (2017) 1–13.
[20] J.B. Kim, Three-dimensional tissue culture models in cancer biology, Semin. Cancer Biol. 15 (2005) 365–377.
[21] F. Urciuolo, A. Garziano, G. Imparato, V. Panzetta, S. Fusco, C. Casale, P.A. Netti, Biophysical properties of dermal building-blocks affect extra cellular matrix assembly in 3D endogenous macrotissue, Biofabrication 8 (2016) 015010.
[22] G. Imparato, F. Urciuolo, C. Casale, P. Netti, The role of microscaffold properties in controlling the collagen assembly in 3D dermis equivalent using modular tissue engineering, Biomaterials 34 (2013) 7851–7861.
[23] V. Brancato, F. Gioiella, M. Profeta, G. Imparato, D. Guarnieri, F. Urciuolo, P. Melone, P. Netti, 3D tumor microtissues as an in vitro testing platform for microenvironmentally-triggered drug delivery systems, Acta Biomater. 57 (2017) 47–58.
[24] V. Brancato, V. Comunanza, G. Imparato, D. Corà, F. Urciuolo, A. Noghero, F. Bussolino, P. Netti, Bioengineered tumoral microtissues recapitulate desmoplastic reaction of pancreatic cancer, Acta Biomater. 49 (2017) 152–166.
[25] F. Gioiella, F. Urciuolo, G. Imparato, V. Brancato, P. Netti, An engineered breast cancer model on a chip to replicate ECM-activation in vitro during tumor progression, Adv. Healthc. Mater. 5 (2016) 3074–3084.
[26] A. Marczak, M. Denel-Bobrowska, A. Rogalska, M. Lukawska, I. Oszczapowicz, Cytotoxicity and induction of apoptosis by formamidinodoxorubicins in comparison to doxorubicin in human ovarian adenocarcinoma cells, Environ. Toxicol. Pharmacol. 39 (2015) 369–383.
[27] Y. Kojima, A. Acar, E.N. Eaton, K.T. Mellody, C. Scheel, I. Ben-Porath, T.T. Onder, Z.C. Wang, A.L. Richardson, R.A. Weinberg, A. Orimo, Autocrine TGF-beta and stromal cell-derived factor-1 (SDF-1) signaling drives the evolution of tumor-promoting mammary stromal myofibroblasts, Proc. Natl. Acad. Sci. USA 107 (2010) 20009–20014.
[28] A. Orimo, P.B. Gupta, D.C. Sgroi, F. Arenzana-Seisdedos, T. Delaunay, R. Naeem, V.J. Carey, A.L. Richardson, R.A. Weinberg, Stromal fibroblasts present in invasive human breast carcinomas promote tumor growth and angiogenesis through elevated SDF-1/CXCL12 secretion, Cell 121 (2005) 335–348.
[29] P. Longati, X. Jia, J. Eimer, A. Wagman, M.R. Witt, S. Rehnmark, C. Verbeke, R. Toftgård, M. Löhr, R.L. Heuchel, 3D pancreatic carcinoma spheroids induce a matrix-rich, chemoresistant phenotype offering a better model for drug testing, BMC Cancer 27 (2013), https://doi.org/10.1186/1471-2407-13-95.

[30] I. Acerbi, L. Cassereau, I. Dean, Q. Shi, A. Au, C. Park, Y.Y. Chen, J. Liphardt, E.S. Hwang, V.M. Weaver, Human breast cancer invasion and aggression correlates with ECM stiffening and immune cell infiltration, Integr. Biol. 10 (2015) 1120–1134.
[31] M.J. Bissell, D. Radisky, Putting tumours in context, Nat. Rev. Cancer 1 (2001) 46–54.
[32] R.O. Hynes, The extracellular matrix: not just pretty fibrils, Science 326 (2009) 1216–1219.
[33] J. Zhang, J. Liu, Tumor stroma as targets for cancer therapy, Pharmacol. Ther. 137 (2013) 200–215.
[34] G. Imparato, F. Urciuolo, P.A. Netti, *In vitro* three-dimensional models in cancer research: a review, Int. Mater. Rev. 60 (2015) 297–311.
[35] G. Mehta, A.Y. Hsiao, M. Ingram, G.D. Luker, S. Takayama, Opportunities and challenges for use of tumor spheroids as models to test drug delivery and efficacy, J. Control Release 2 (2012) 192–204.
[36] P. Cirri, P. Chiarugi, Cancer-associated-fibroblasts and tumour cells: a diabolic liaison driving cancer progression, Cancer Metastasis Rev. 31 (2012) 195–208.
[37] A.K. Clark, A.V. Taubenberger, R.A. Taylor, B. Niranjan, Z.Y. Chea, E. Zotenko, Shirly Sieh, J.S. Pedersen, S. Norden, M. Frydenberg, A bioengineered microenvironment to quantitatively measure the tumorigenic properties of cancer-associated fibroblasts in human prostate cancer, Biomaterials 34 (2013) 4777–4785.
[38] Q. Wu, Z. Yang, Y. Nie, Y. Shi, D. Fan, Multi-drug resistance in cancer chemotherapeutics: mechanisms and lab approaches, Cancer Lett. 347 (2014) 159–166.
[39] G. Mehta, A.Y. Hsiao, M. Ingram, G.D. Luker, S. Takayama, Opportunities and challenges for use of tumor spheroids as models to test drug delivery and efficacy, J. Control Release 164 (2012) 192–204.
[40] Winner K. Kanigel, M.P. Steinkamp, R.J. Lee, M. Swat, C.Y. Muller, M.E. Moses, Y. Jiang, B.S. Wilson, Spatial modeling of drug delivery routes for treatment of disseminated ovarian cancer, Cancer Res. 15, 76(6) (2016 March) 1320–1334, https://doi.org/10.1158/0008-5472.CAN-15-1620.
[41] R.H. Grantab, I.F. Tannock, Penetration of anticancer drugs through tumor tissue as a function of cellular adhesion and packing density of tumor cells, BMC Cancer 12 (2012).
[42] R.E. Durand, Slow penetration of anthracyclines into spheroids and tumors: a therapeutic advantage?, Cancer Chemother Pharmacol. 26 (1990) 198–204.
[43] I.K. Choi, R. Strauss, M. Richter, C.O. Yun, A. Lieber, Strategies to increase drug penetration in solid tumors, Frontiers in oncology 3 (2013) 193.
[44] M.T. Santini, G. Rainaldi, P.L. Indovina, Apoptosis, cell adhesion and the extracellular matrix in the three-dimensional growth of multicellular tumor spheroids, Crit. Rev. Oncol. Hematol. 36 (2000) 75–87.
[45] N. Sawada, M. Murata, K. Kikuchi, M. Osanai, H. Tobioka, T. Kojima, Hideki Chiba, Tight junctions and human diseases, Med. Electron Microsc. 36 (2003) 147–156.
[46] A. Tőkés, J. Kulka, S. Paku, Á. Szik, C. Páska, P.K. Novák, L. Szilák, A. Kiss, K. Bögi, Z. Schaff, Laudin-1,-3 and-4 proteins and MRNA expression in benign and malignant breast lesions: a research study, Breast Cancer Res. 7 (2005) 296–305.
[47] T.A. Martin, G. Watkins, R.E. Mansel, W.G. Jiang, Loss of tight junction plaque molecules in breast cancer tissues is associated with a poor prognosis in patients with breast cancer, Eur. J. Cancer 40 (2004) 2717–2725.
[48] A. Taherian, X. Li, Y. Liu, T.A. Haas, Differences in integrin expression and signaling within human breast cancer cells, BMC Cancer 11 (2011) 293.
[49] I.M. Adjei, S. Blanka, Modulation of the tumor microenvironment for cancer treatment: a biomaterials approach, J. Funct. Biomater. 6 (2015) 81–103.
[50] C. Fischbach, H.J. Kong, S.X. Hsiong, M.B. Evangelista, W. Yuen, D.J. Mooney, Cancer cell angiogenic capability is regulated by 3D culture and integrin engagement, Proc. Natl. Acad. Sci. 106 (2009) 399–404.
[51] G.L. Scheffer, M. Kool, M. Heijn, M. de Haas, A.C.L.M. Pijnenborg, J. Wijnholds, A. van Helvoort, M.C. de Jong, J.H. Hooijberg, C.A.A.M. Mol, M. van der Linden, J. L. de Vree, P. van der Valk, R.P.J. Oude Elferink, P. Borst, R.J. Scheper, Specific Detection of multidrug resistance proteins MRP1, MRP2, MRP3, MRP5, and MDR3 P-glycoprotein with a panel of monoclonal antibodies, Cancer Res. 60 (2000) 5269–5277.
[52] M.M. Gottesman, T. Fojo, S.E. Bates, Multidrug resistance in cancer: role of ATP-dependent transporters, Nature 2 (2002) 48–58.
[53] R. Barrera-Rodríguez, J. Fuentes, Multidrug resistance characterization in multicellular tumour spheroids from two human lung cancer cell lines, Cancer Cell Int. 15 (2015) 1–11.
[54] G. Imparato, C. Casale, S. Scamardella, F. Urciuolo, M. Bimonte, F. Apone, P.A. Netti, A novel engineered dermis for in vitro photodamage research, J. Tissue Eng. Regen. Med. 11 (2017) 2276–2285.